Seizures, spreading depolarizations and sudden death

Jansen, N.A.

Chapter 8

Impaired θ-γ coupling indicates inhibitory dysfunction and seizure risk in a Dravet syndrome mouse model

Nico A. Jansen
Carlos Perez
Maarten Schenke
Anouk W. van Beurden
Anisa Dehghani
Rob A. Voskuyl
Roland D. Thijs
Ghanim Ullah
Arn M.J.M. van den Maagdenberg
Else A. Tolner

J Neurosci 2021;41(3):524-537

ABSTRACT

Dravet syndrome (DS) is an epileptic encephalopathy that still lacks biomarkers for epileptogenesis and its treatment. Dysfunction of $Na_V1.1$ sodium channels, which are chiefly expressed in inhibitory interneurons, explains the epileptic phenotype. Understanding the network effects of these cellular deficits may help predict epileptogenesis. Here, we studied theta-gamma coupling as a potential marker for altered inhibitory functioning and epileptogenesis in a DS mouse model. We found that cortical theta-gamma coupling was reduced in both male and female juvenile DS mice and persisted only if spontaneous seizures occurred. Theta-gamma coupling was partly restored by cannabidiol. Locally disrupting $Na_V1.1$ expression in the hippocampus or cortex yielded early attenuation of theta-gamma coupling, which in the hippocampus associated with fast ripples, and which was replicated in a computational model when voltage-gated sodium currents were impaired in basket cells. Our results indicate attenuated theta-gamma coupling as a promising early indicator of inhibitory dysfunction and seizure risk in DS.

INTRODUCTION

Dravet syndrome (DS) is an epileptic encephalopathy characterized by early-onset seizures, followed by severe cognitive and behavioral deficits.[1, 2] The majority of DS cases result from a heterozygous loss-of-function mutation in the *SCN1A* gene, which encodes the pore-forming α1 subunit of voltage-gated sodium channel type 1 ($Na_V1.1$). In mice with a heterozygous knock-out of *Scn1a*, core clinical features of DS including spontaneous seizures,[3] cognitive deficits and autism-related behavior[4] are replicated. Voltage-dependent sodium currents are reduced in GABAergic inhibitory interneurons, whilst unaffected in hippocampal pyramidal neurons of DS mice.[3] In the hippocampus and cortex, $Na_V1.1$ is mostly expressed in interneurons[5] and loss of $Na_V1.1$ function in inhibitory populations is sufficient to reproduce the epileptic phenotype of DS mice.[6] These studies thus implicate loss of inhibitory functioning in DS pathophysiology.

How loss of $Na_V1.1$ function affects network dynamics, however, remains unclear, while such knowledge is crucial to understanding epileptogenesis and cognitive deficits. Although excitability of cortical inhibitory interneurons was decreased in brain slices of DS mice, *in vivo* cortical local field potential (LFP) and spontaneous interneuron firing appeared unaffected.[7] Fast-spiking parvalbumin-positive interneurons, a class of inhibitory interneurons that is affected in DS mice,[7, 8] importantly contribute to LFP gamma oscillations.[9, 10] Parvalbuminergic neurons show a particularly high propensity to fire phase-locked to theta oscillations in the hippocampus[11] and cortex,[12] suggesting a key role of these interneurons in theta-gamma cross-frequency coupling.[9] Coupling of gamma oscillations to theta rhythm is indeed decreased when synaptic inhibition onto parvalbumin-positive neurons is impaired.[13] Recently, local loss of hippocampal $Na_V1.1$ function was shown to impair inhibitory firing and coupling of gamma amplitude to theta phase in rats.[14] How this relates to seizure development, hippocampal and cortical dynamics in DS mice, however, remains to be explored.

Here, we studied spontaneous cortical network dynamics during development in DS mice for early changes in theta or gamma oscillations and their cross-frequency phase-amplitude coupling. By inducing local heterozygous or homozygous knock-out of *Scn1a* in the hippocampus or cortex, we addressed the effect of partial or total ablation of $Na_V1.1$, respectively, within these structures on network dynamics in relation to seizure development. We found that theta-gamma coupling was decreased in DS mice compared to wildtype, which, also upon local ablation of $Na_V1.1$, preceded seizure activity. Decreased theta-gamma coupling persisted only in animals with spontaneous seizures, and associated with hippocampal fast ripples. In a computational hippocampal network model, loss of voltage-gated sodium currents in inhibitory neurons reproduced the main experimental findings, including a pronounced impairment of theta-gamma coupling. These results suggest that theta-gamma coupling may serve as an early indicator of inhibitory dysfunction and seizure risk in DS.

MATERIALS AND METHODS

Animals

Mice with a deletion of exon 8 of the *Scn1a* gene were created as described previously.[15] These global *Scn1a*$^{-/+}$ mice (referred to as "DS mice") were backcrossed to C57BL/6J mice for at least 5 generations. Both male and female DS mice and wildtype (WT) littermates were used for experiments. In the conditional *Scn1a* mouse line, exon 8 of the *Scn1a* gene is flanked by LoxP sites,[15] which allows for region-specific ablation after exposure to Cre recombinase. Heterozygous and homozygous floxed (*Scn1a*$^{fl/+}$ or *Scn1a*$^{fl/fl}$, respectively) mice and WT littermates were used for the viral injection experiments. Animals had free access to food and water and were kept under standard housing conditions (temperature of 22 ± 1.5°C, 12-hour light/dark cycle). All experiments were approved by local and national ethical committees following recommendations of the European Communities Council Directive (2010/63/EU) and carried out in accordance with ARRIVE guidelines.

Surgery and viral infection

For chronic recordings in DS mice and WT littermates, local-field potential (LFP) electrodes (75 µm platinum/iridium; PT6718, Advent Research Materials, Oxford, UK) were implanted at P20-21 under isoflurane anesthesia (induction 4%; maintenance 1.5%). Electrodes were implanted in primary visual cortex (V1; -3.5 anteroposterior [AP], ±2.4 mediolateral [ML], -0.5 dorsoventral [DV]; mm relative to bregma) and primary motor cortex (M1; +1.5 AP, ±1.8 ML, -0.5 DV). A subset of WT and DS mice was implanted with an additional LFP electrode in the right dorsal hippocampus (-2.0 AP, +2.2 ML, -1.4 DV).

To induce local knock-out of *Scn1a*, an AAV vector expressing mCherry-Cre under the EF1α-promotor (viral prep # 55632, a gift from Karl Deisseroth, Addgene, Watertown, MA) was injected in P42-56 *Scn1a*$^{fl/+}$ and *Scn1a*$^{fl/fl}$ mice. Injections (500 nL per injection, 50 nL/min) were made bilaterally in dorsal (-2.0 AP, ±2.2 ML, -1.4 DV) and ventral (-3.0 AP, ±3.1 ML, -2.6 DV) hippocampus, or in V1, followed by implantation of LFP electrodes. For cortically injected animals, LFP electrodes were implanted in V1 and M1. The use of heterozygous and homozygous floxed mice was predicted to result in a partial and total ablation of $Na_V1.1$ following local expression of Cre, respectively. WT littermates that underwent the same procedure served as controls. For cortical injections, in a subset of *Scn1a*$^{fl/+}$ mice, a different AAV vector was used (expressing eGFP-Cre; viral prep #105545, a gift from James M. Wilson, Addgene) to allow comparison with previously published data.[15]

Pharmacology

Cannabidiol (Tocris, Bristol, UK) was dissolved in DMSO, which was diluted in a vehicle solution (5% DMSO: 5% cremophor: 90% saline) immediately prior to injection. P35-36 DS mice received an intraperitoneal (i.p.) injection of cannabidiol (100 mg/kg body weight) or vehicle on two consecutive days between 8-10 A.M., in a randomized fashion and by an experimenter blinded to the treatment.

Immunohistochemistry

After experiments, animals were euthanized by CO_2 and transcardially perfused with phosphate-buffered saline (PBS) and 4% paraformaldehyde. Following removal and post-fixation of brain tissue, coronal sections (20 μm) were prepared. Sections were heated in 10 mmol/L sodium citrate buffer with 0.05% Tween for 10 minutes at 80°C. Subsequently, a blocking solution containing 10% normal goat serum was applied, and sections were incubated in rabbit anti-$Na_V1.1$ (1:200; Alomone Labs, Jerusalem, Israel), followed by incubation in goat anti-rabbit Cy2 (1:200; Jackson Immunoresearch, Cambridgeshire, UK). Mounting was performed in glycerol/PBS (1:1) containing 12.5 mg/mL sodium azide and 1 μL/mL Hoechst-33258. Sections were examined using an epifluorescence or confocal microscope with appropriate filter sets.

Data acquisition and analysis

DS mice and WT littermates were videotaped from P18-19 in a PhenoTyper® home cage (Noldus, Wageningen, the Netherlands) to allow detection of early spontaneous seizures, until the day of surgery at P20-21. Immediately after surgery, both these mice and virally injected mice were connected to a 7-channel commutator in a Faraday cage for continuous recordings of LFP and video. Signals were pre-amplified (3X), filtered (0.05-500 Hz) and amplified (200X and 400X for hippocampal and cortical recordings, respectively) using custom-build hardware, and digitized at 5 kHz (Power 1401 and Spike2 software, CED, Cambridge, UK). All LFP recordings were *post hoc* inspected for epileptiform activity. The Racine scale[16] was used for scoring of behavior from video recordings during discharges that lasted >5 seconds. Seizures that progressed to stage 3-5 were included in analyses, as these seizures could also be reliably detected when only video recordings were available (i.e. for P18-21 mice). For detection of interictal spikes (IIS) following local knock-out of *Scn1a*, local LFP power in the 30-100 Hz range was calculated every 24 hours for 1 hour of non-REM sleep, a vigilance state during which IIS are prevalent in DS mice.[17] Candidate events exceeding a threshold of 3 SDs of signal were visually inspected, and animals were considered showing IIS if >5 IIS were observed during the analyzed 1-hour window on that day. To detect fast ripples, hippocampal LFP recordings were bandpass filtered (infinite impulse response Butterworth filter of 2nd order) between 200-600 Hz and candidate events were detected by thresholding (>10 SDs), which effectively distinguished fast ripples from IIS. Only events that occurred during behavioral immobility – assessed from the reference signal and locomotor activity recorded by an infrared motion detection sensor in the Faraday cage – were visually inspected, as muscle artifacts were often found in the 200-600 Hz frequency range during active wakefulness.

To assess cortical network dynamics during REM sleep and active wakefulness, LFP recorded during the morning (6-12 A.M.) was analyzed, starting at P23, allowing 2-3 days of habituation to the recording setup. Vigilance state was determined per 5-second epoch using V1 LFP, the reference signal and locomotor activity recorded by the infrared motion detection sensor. Epochs during seizures and/or postictal periods (1 hour after the end of a seizure) were excluded from further analyses. REM sleep was defined by a theta (5-10 Hz) to delta (1-4 Hz) power ratio of

>2.5, in the absence of locomotor activity or motion artifacts. Active wakefulness was defined by a theta-delta power ratio of >2 during epochs containing locomotor activity and/or high variance in the reference signal. Epochs were artifact-rejected, low-pass-filtered (Chebyshev IIR eighth-order filter) and down-sampled to 1 kHz. A total of 10 minutes of randomly selected epochs was used for further analyses. Power spectra were computed by applying a Hamming window over each epoch, followed by a fast Fourier transform and averaging of the resulting power spectra. Phase-amplitude coupling was assessed using a measure referred to as the modulation index (MI), calculated as described previously.[18] In short, LFP epochs were bandpass-filtered for phase (3-14 Hz, 2-Hz bandwidths, steps of 1 Hz) and amplitude (40-200 or 40-300 Hz, 4-Hz bandwidths, steps of 2 Hz) frequencies. The Hilbert transform was applied to extract phase and amplitude information. Each phase frequency was binned in 18 bins of 20°, and mean amplitude per amplitude frequency was calculated inside each bin. A distribution was subsequently obtained by normalization of the mean amplitude in each phase bin by the sum over all bins. To compare the resulting phase-amplitude distribution with a uniform distribution, the Kullback-Leibler distance was calculated. The MI was obtained by normalizing this metric to the logarithm of the number of phase bins. For group analyses, theta-gamma coupling was expressed in a single value by averaging over all theta and gamma frequencies, or over specific gamma bands, as indicated. All analyses were performed using custom-written MATLAB (versions used: 2018b and 2019b, MathWorks, Natick, MA) scripts.

Computer modeling

The basic equations for the membrane potential of individual neurons and various ion channels were adopted from.[19] The model network consists of 5 pyramidal cells (EX), 5 oriens-lacunosum moleculare (OLM) interneurons, and 5 fast-spiking basket cell (BC) interneurons, with all-to-all connections. We noticed that increasing the network size did not change the conclusions from the model as long as the synaptic connections were properly scaled (not shown). The equations for individual cells were modified and extended to incorporate the dynamics of various ion species in the intra- and extracellular spaces of the neurons and neurotransmitter homeostasis using a formalism previously developed.[20-22] Full details about the model are given in Figure 10-1. Here, we describe the main equations.

The membrane potential, V_m, of each EX, BC, and OLM neuron in the network is controlled by various Na^+ (I_{Na}), K^+ (I_K), and Cl^- (I_{Cl}) currents, Na^+ and K^+ currents due to the Na^+/K^+-ATPase (I_{pump}), and random inputs from neurons that were not a part of the network, modeled as a Gaussian distribution (I_{stoch}), that is

$$C_m \frac{d V_m^{EX,BC,OLM}}{dt} = I_{Na}^{EX,BC,OLM} + I_K^{EX,BC,OLM} + I_{Cl}^{EX,BC,OLM} + I_{stoch}^{EX,BC,OLM} \quad (1)$$

where C_m is the membrane capacitance and superscripts *EX*, *BC*, and *OLM* correspond to pyramidal, basket cell, and OLM neurons, respectively. Various currents used for the different neuron types are given in the section "Membrane Potential" of Figure 10-1.

To model the dynamics of various ionic species, we considered the extracellular space (ECS) as a separate compartment surrounding each cell. Each neuron exchanged ions with its ECS compartment through active and passive currents, and the Na^+/K^+-ATPase. The ECS compartment can also exchange K^+ with the glial compartment, and perfusion solution (or vasculature in intact brain).[20, 23-25] Including diffusion of ions between the ECS compartments of neighboring neurons did not affect the results, and were therefore ignored.

The change in extracellular K^+ concentration ($[K^+]_o$) is a function of I_K, I_{pump}, uptake by glia surrounding the neuron (I_{glia}), and the diffusion between the neuron and bath perfusate (I_{diff}).

$$\frac{d[K^+]_o}{dt} = -\gamma\beta I_K - 2\gamma\beta I_{pump} + I_{glia} - I_{diff} \qquad (2)$$

Where β is the ratio of intracellular space (ICS) to ECS. $\gamma = A_m^{(n)} \times 10^4/(F \times \omega_i)$ is the conversion factor from current units to flux units. F, $A_m^{(n)}$, and ω_i are the Faraday's constant, surface area of the neuron, and intracellular volume of the neuron, respectively. The factor 2 in front of I_{pump} is due to the fact that the Na^+/K^+ pump extrudes two K^+ in exchange for three Na^+ ions.

The rate of change of intracellular Na^+ concentration ($[Na^+]_i$) is controlled by I_{Na} and I_{pump},[20] that is

$$\frac{d[Na^+]_i}{dt} = -\gamma I_{Na} - 3\gamma I_{pump} \qquad (3)$$

The fluxes used in equations (2) and (3) are listed in section "Ion Concentrations" of Figure 10-1. The concentrations of intracellular K^+ ($[K^+]_i$), intracellular Cl^- ($[Cl^-]_i$), extracellular Na^+ ($[Na^+]_o$), and extracellular Cl^- ($[Cl^-]_o$) are given by conservation laws and are also listed in the same section.

In addition to ion concentration dynamics, our model also incorporates the details of neurotransmitter homeostasis. Glutamate and GABA in the synaptic cleft and ECS are regulated by i) spiking-related release from EX (for glutamate), and BC and OLM (for GABA), ii) uptake by pre- and postsynaptic neurons and glia through glutamate and GABA transporters, iii) diffusion between the cleft and ECS, and iv) the recycling into releasable pools. The model also includes the binding and unbinding of glutamate to NMDA and AMPA receptors, and GABA to $GABA_A$ receptors, and the currents due to these receptors. Details of the equations are given in the section "Neurotransmission" of Figure 10-1.

The LFP is modeled by considering a non-spiking pyramidal neuron in the network as described in.[19] This neuron receives the same synaptic inputs as the active pyramidal neurons in the network, but it does not generate action potentials due to the absence of the main currents responsible for action potential generation. The model LFP thus reflects subthreshold voltage changes in the EX-cell population. Similar to the *in vivo* data analysis, 10 minutes of simulated LFP data were used to obtain power spectra and phase-amplitude coupling metrics, as described earlier.

Experimental design and statistical analysis

Data from 89 mice were included, including 15 WT and 26 DS mice for video-EEG recordings, 9 DS mice for pharmacological experiments, and 13 WT, 14 *Scn1a*$^{fl/+}$ and 12 *Scn1a*$^{fl/fl}$ mice for AAV vector injections. Data are presented as mean ± SEM, unless indicated otherwise. Statistical testing was conducted in MATLAB or GraphPad Prism (GraphPad Software, La Jolla, CA). Based on whether data were paired and their distribution normality, which was assessed by the Anderson-Darling test, data were compared using the Welch's *t*-test, paired *t*-test, Mann-Whitney test or Wilcoxon test for single comparisons. For multiple comparisons, a one or two-way ANOVA with Tukey's test, repeated-measures ANOVA with Dunnett's test or Kruskal-Wallis with Dunn's test was used. Sample sizes were not based on statistical methods, but instead informed by those frequently used in the field. $p < 0.05$ was considered to indicate significance.

RESULTS

Modulation of cortical gamma amplitude by theta phase is attenuated in juvenile DS mice

Cortical LFP and video were recorded in freely behaving *Scn1a*$^{-/+}$ (DS) and wildtype (WT) mice starting from P20-21. Modulation of cortical gamma oscillations by theta rhythm is low during vigilance states lacking prominent theta oscillations, i.e. during quiet wakefulness and non-REM sleep.[26] We therefore limited our analyses to epochs during vigilance states with prominent cortical theta oscillations, i.e. REM sleep (examples in Fig. 1A) and active wakefulness. Average V1 LFP power spectral density for theta (5-10 Hz), low gamma (40-90 Hz) and high gamma (90-160 Hz) frequencies during REM sleep at P23 was similar between genotypes (Fig. 1B,C), although a decrease in theta peak frequency was observed in DS mice (Fig. 1D). Comodulogram analyses of V1 LFP in WT mice showed that theta phase modulated the amplitude of low and high gamma (Fig. 1E). Although this pattern was also present in DS mice, the modulation of gamma power by theta phase was significantly impaired for both frequency ranges (Fig. 1F). The theta phase at which gamma amplitude peaked was similar between genotypes, with high gamma peaking significantly later in the theta cycle than low gamma for both WT and DS mice (Fig. 1G,H). Average REM sleep duration was similar between WT and DS mice (48.9 ± 4.2 s and 46.6 ± 3.0 s, respectively; $t_{(26)} = 0.45$, $p = 0.66$, *t*-test), thereby excluding changes in REM sleep duration as a potential cause for impaired theta-gamma coupling strength.[27] Similar results were obtained from epochs during active wakefulness (Fig. 2), although in both WT and DS mice modulation of high gamma oscillations was largely absent, and modulation of both low and high gamma frequencies was lower when compared to REM sleep (Fig. 2F-I). These data indicate that cortical theta-gamma coupling is attenuated in juvenile DS mice, which cannot be explained by changes in theta or gamma power.

FIGURE 1A-1E. Dravet syndrome (DS) mice display decreased cortical theta-gamma cross-frequency coupling at P23.

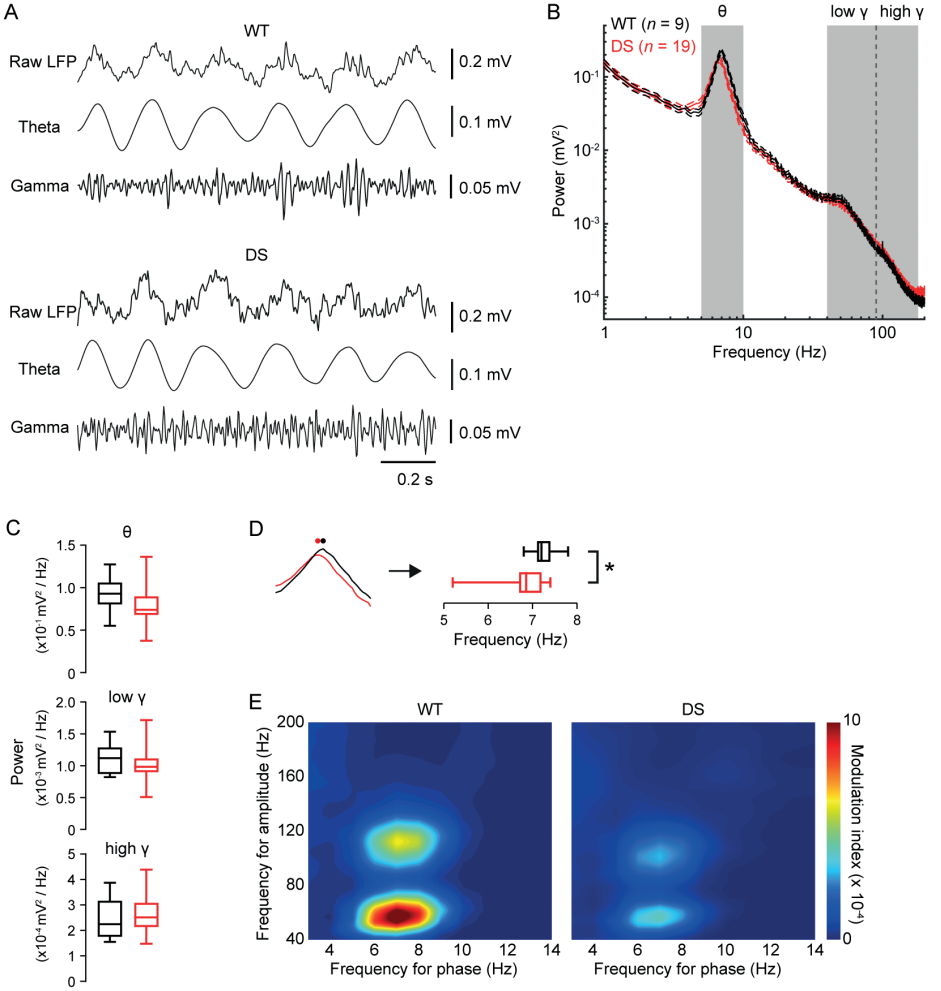

(A) Example traces of raw, theta-filtered (5-10 Hz) and gamma-filtered (40-160 Hz) LFP in the primary visual cortex (V1) during REM sleep in a wildtype (WT) and DS mouse. **(B)** Average V1 LFP power spectra during REM sleep in WT (black) and DS (red) mice. Peak theta frequency was significantly reduced in DS mice (**C**; detail of mean power in theta range, black and red dots indicate average peak theta frequency; $t_{(27)} = 2.5$, $^*p = 0.020$, Welch's *t*-test). **(D)** No significant differences in power were present between genotypes within theta (θ), low (40-90 Hz) or high gamma (γ; 90-160 Hz) frequency ranges. **(E)** Average phase-amplitude comodulograms of V1 during REM sleep in WT ($n = 9$) and DS ($n = 19$) mice at P23

FIGURE 1F-1H. Dravet syndrome (DS) mice display decreased cortical theta-gamma cross-frequency coupling at P23.

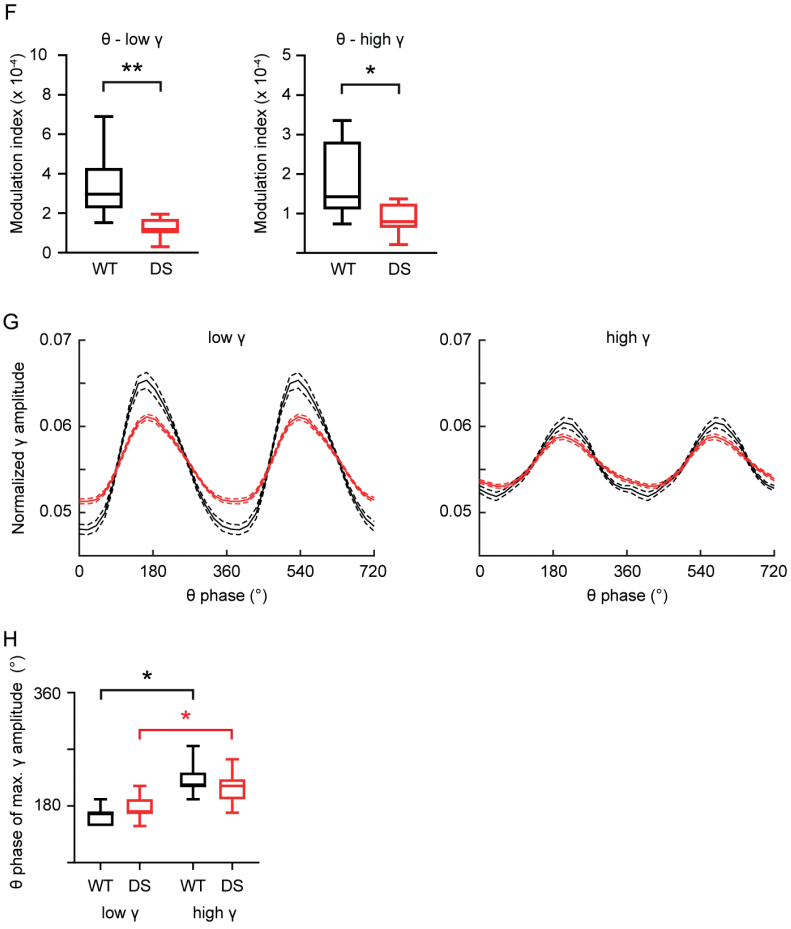

(F) Theta-gamma coupling was significantly reduced in DS mice, for both low and high gamma frequencies ($t_{(8,9)}$ = 3.8 and $t_{(9.2)}$ = 2.9, respectively, *p = 0.019 and **p = 0.004, Welch's t-test). **(G)** Normalized gamma amplitude per 20° phase bin of the theta cycle for V1 during REM sleep. No significant differences were present between WT and DS mice. **(H)** High gamma amplitude peaked significantly later in the theta cycle than low gamma in both genotypes (*p < 0.005, Wilcoxon test).

FIGURE 2. Deficient cortical theta-gamma coupling during active wakefulness in Dravet syndrome (DS) mice.

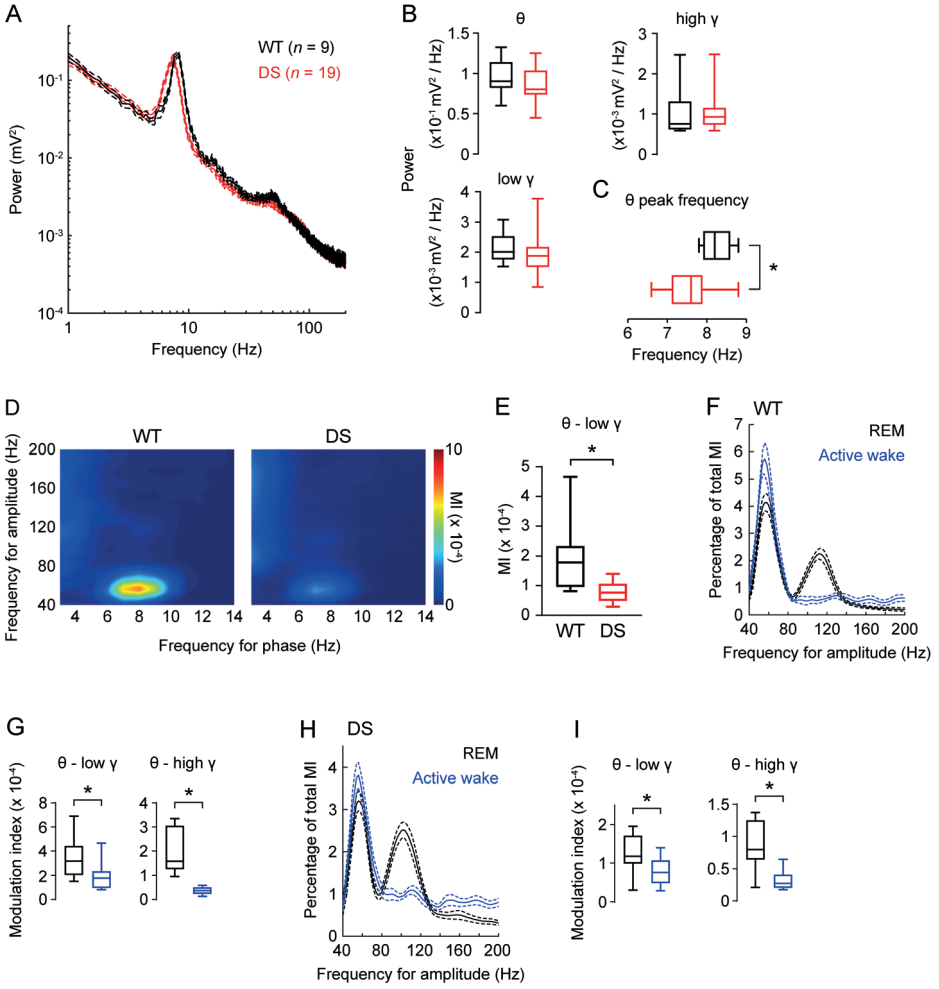

(A) Average primary visual cortex (V1) LFP power spectra during wakefulness in wildtype (WT; black) and DS (red) mice. No significant differences were present between genotypes in power within theta (θ; 5-10 Hz), low gamma (γ; 40-90 Hz) or high gamma (90-160 Hz) frequency ranges **(B)**. **(C)** Peak theta frequency was significantly reduced in DS mice ($t_{(22.7)}$ = 3.5, *p = 0.002, Welch's t-test). **(D)** Average phase-amplitude comodulograms of V1 LFP during active wakefulness in WT (n = 9) and DS (n = 19) mice at P23. **(E)** Theta-low gamma coupling was significantly reduced in DS mice ($t_{(7.9)}$ = 2.7, *p = 0.030, Welch's t-test). For both WT **(F,G)** and DS **(H,I)** mice, theta modulation of gamma amplitude was largely limited to low gamma frequencies during active wakefulness, while modulation of both low and high gamma frequencies was lower when compared to REM sleep.

Impaired theta-gamma coupling in the hippocampus of juvenile DS mice

Previous studies indicate that theta oscillations recorded in the neocortex are volume-conducted currents originating from the hippocampus.[12, 28] The hippocampus, a brain region that importantly contributes to the epileptic phenotype of DS mice,[15, 29, 30] also displays theta-gamma phase-amplitude coupling.[31, 32] To establish whether hippocampal theta-gamma coupling is disturbed in DS mice, we assessed hippocampal LFP in WT (n = 6) and DS (n = 7) mice during REM sleep at P23. Similar to results obtained from V1, theta and gamma power were not significantly different between genotypes (Fig. 3A,B), whereas theta peak frequency was reduced in DS mice (inset Fig. 3A). Variability in gamma power and theta-gamma coupling appeared increased when compared to cortical LFP, which may be explained by slight variations in electrode position within the hippocampus since patterns of theta-gamma coupling are different among hippocampal sublayers.[33] Hippocampal theta-gamma coupling was, however, robustly decreased in DS mice (Fig. 3C,D).

FIGURE 3. Deficient theta-gamma coupling in the hippocampus of Dravet syndrome (DS) mice.

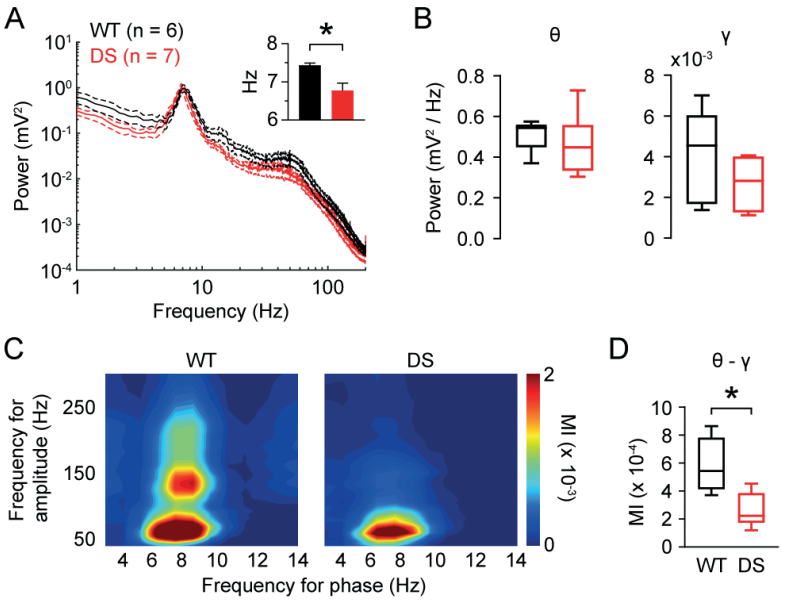

(A) Power spectral density of LFP recorded in the dorsal hippocampus during REM sleep in wildtype (WT; black) and DS (red) mice. Peak theta frequency was significantly reduced in DS mice (inset; $t_{(6.9)}$ = 3.2, *p = 0.011, Welch's t-test). No significant differences were present between genotypes in power within theta (θ; 5-10 Hz) and gamma (γ; 40-300 Hz) frequency ranges **(B)**. **(C)** Average phase-amplitude comodulograms of the same LFP signals. MI, modulation index. **(D)** Theta-gamma coupling was significantly reduced in DS mice ($t_{(8.1)}$ = 3.64, *p = 0.006, Welch t-test).

Cortical theta-gamma coupling normalizes in DS mice without spontaneous seizures

The profound cortical theta-gamma coupling (for both low and high gamma) observed during REM sleep led us to limit subsequent analyses to this vigilance state. First, we assessed whether developmental changes in cortical theta-gamma coupling occurred over the 3-week recording period by analyzing V1 LFP during REM sleep at 2, 7, 14 and 21 days after surgery (i.e. postnatal day 23, 28, 35 and 42; Fig. 4). Theta-gamma coupling increased over this period in both WT and DS mice (Fig. 4A,B). Similar to the observations at P23, DS mice showed decreased theta-gamma coupling when compared to WT mice at P42 (MI values of $5.2 \pm 0.7 \times 10^{-4}$ and $10.4 \pm 1.5 \times 10^{-4}$, respectively; calculated for the total gamma range [40-160 Hz]; $t_{(11)} = 3.2$, $p = 0.009$, Welch's t-test).

The recording period included postnatal week 4, during which spontaneous seizures are most prevalent in DS mice.[34] Accordingly, here, spontaneous seizures in DS mice were most often detected between P21-28 (Fig. 4C). Three DS mice had a fatal seizure (during P24-26), whereas a subset of DS mice (7 out of 19) remained seizure-free over the 3-week recording period. As early seizures, induced by hyperthermia or a chemoconvulsant, were shown to aggravate the epileptic phenotype and cognitive deficits in a knock-in DS mouse model,[35] we assessed whether theta-gamma coupling progressed differently in DS mice that did or did not express seizures during the recording period. Although seizure-free DS mice did show a decrease in cortical theta-gamma coupling for both low and high gamma at baseline (P23), no significant differences were present at P28, P35 and P42 in these mice compared to WT littermates (Fig. 4D). In contrast, theta-gamma coupling was persistently decreased, for both low and high gamma, in DS mice that showed at least one seizure during the 3-week recording period (seizure count per mouse: 5.1 ± 1.5, range 1-19), when compared to WT mice (Fig. 4D).

Decreased progression of cortical theta-gamma coupling in DS mice is improved by cannabidiol

To test whether antiseizure drug treatment could improve attenuated cortical theta-gamma coupling, a separate group of DS mice ($n = 9$) was used to assess the effects of cannabidiol (CBD). CBD decreased seizure frequency in patients with Dravet syndrome,[36] while in DS mice it decreased seizure frequency and severity and increased inhibitory neurotransmission in the hippocampus.[37] Here, in DS mice, the progression of cortical theta-gamma coupling ceased after P35, contrasting the steady progression of theta-gamma coupling observed in WT mice (Fig. 5A,B). DS mice received a single i.p. injection of cannabidiol (CBD; 100 mg/kg) or vehicle at P35 using a randomized crossover design at an interval of 24 hours. Theta-gamma coupling was assessed in V1 LFP during REM sleep up to 5 hours after i.p. injection, during which plasma and brain CBD levels are high in mice.[38] When compared to vehicle, acute treatment of DS mice with CBD resulted in a modest but consistent increase in theta-gamma coupling (Fig. 5C,D).

FIGURE 4. Persistently reduced cortical theta-gamma coupling in Dravet syndrome (DS) mice that show spontaneous seizures.

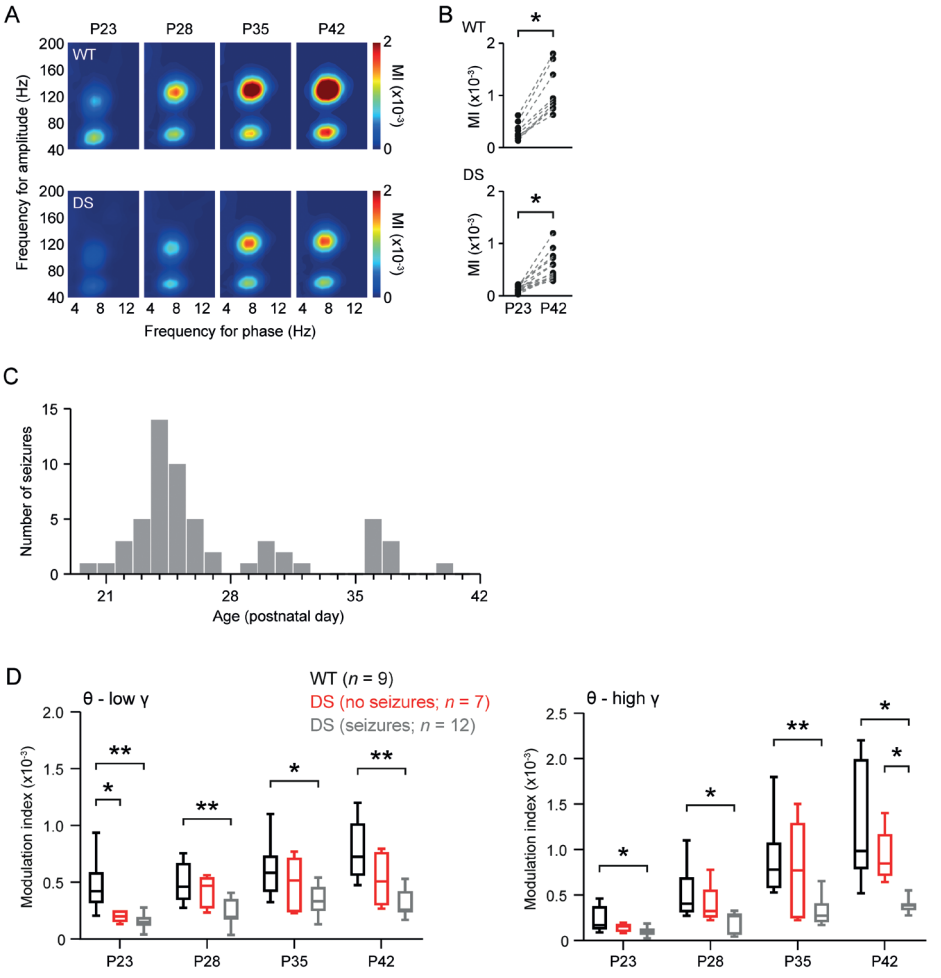

(A) Average phase-amplitude comodulograms of primary visual cortex (V1) showing progression of cortical theta-gamma coupling during postnatal week 4-7. **(B)** Average modulation index (MI), calculated for theta (5-10 Hz) and total gamma (40-160 Hz), was markedly increased in both wildtype (WT) and DS mice at P42, when compared to P23 ($t_{(8)}$ = 7.0 and $t_{(15)}$ = 6.4, respectively, *p < 0.0001, paired t-test). **(C)** Total frequency of spontaneous seizures in DS mice (n = 19). A subset of DS mice (n = 3) died during the recording period, between P24-26. **(D)** Progression of cortical theta-gamma cross-frequency coupling for WT (black) and DS mice with (grey) and without (red) spontaneous seizures over the recording period. Note that at P23 the MI was significantly decreased compared to WT for both groups of DS mice, while at later ages this decrease was maintained only in DS mice with seizures for both low (40-90 Hz) and high (90-160 Hz) gamma ($F_{(2,22)}$ = 9.5, *p < 0.05, **p < 0.005, repeated-measures ANOVA with Tukey's test).

FIGURE 5. Acute treatment with cannabidiol (CBD) improves progression of theta-gamma coupling in Dravet syndrome (DS) mice.

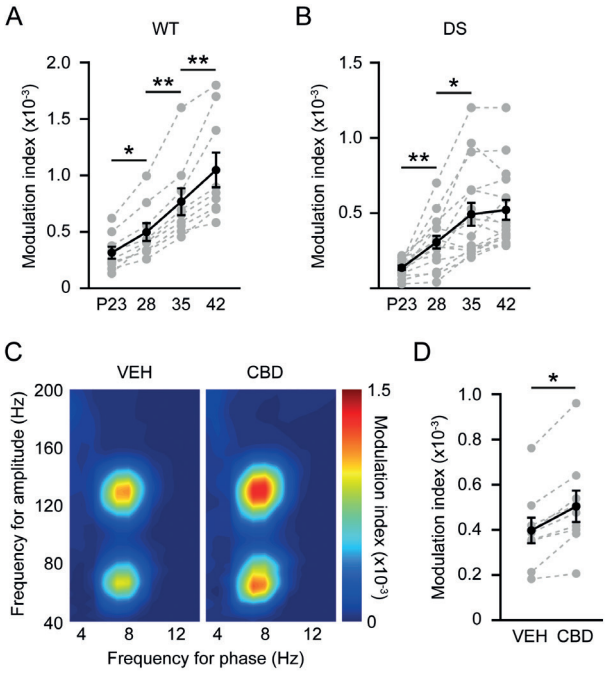

Wildtype (WT) mice showed steady progression of average theta-gamma cross-frequency coupling over time (**A**; calculated for total gamma [40-160 Hz]; $F_{(3,8)} = 15.5$), while for DS mice progression stagnated after P35 (**B**; $F_{(3,15)} = 27.5$, $*p < 0.05$, $**p < 0.005$, repeated-measures ANOVA with Tukey's test). Note that analyses presented in A and B are performed on the same groups as included in Figure 2, excluding DS mice that died during the recording ($n = 3$). **(C)** Average phase-amplitude comodulograms of primary visual cortex (V1) following treatment with vehicle (VEH) or CBD (100 mg/kg) in DS mice between P35-42. **(D)** Average modulation index (MI), calculated for theta (5-10 Hz) and total gamma (40-160 Hz), was significantly increased following treatment with CBD ($t_{(8)} = 5.1$, $*p = 0.0009$, ratio paired *t*-test).

Attenuation of cortical theta-gamma coupling precedes seizures following hippocampal-specific knock-out of *Scn1a*

The early attenuation of cortical theta-gamma coupling that was observed in DS mice at P23 occurred regardless of the epileptic phenotype. Thus, the deficit in cross-frequency coupling may be directly related to the inhibitory dysfunction caused by impaired sodium currents in the DS model.[3] Alternatively, attenuated coupling may result from a secondary effect of inhibitory dysfunction on cortical connectivity during critical period plasticity.[39, 40] We aimed to address this issue by introducing the *Scn1a* defect at adult age, using local brain injections of an AAV vector expressing mCherry-Cre in P42-56 mice in which exon 8 of the *Scn1a* gene is floxed by LoxP sites (in one or both copies of the gene, i.e. $Scn1a^{fl/+}$ or $Scn1a^{fl/fl}$, respectively). This approach additionally allowed assessment of the effects of brain region-specific $Na_V1.1$ dysfunction on theta-gamma coupling.

Hippocampal ablation of $Na_V1.1$ results in an increased susceptibility to seizures.[15, 30] Here, we studied the effect of exposure to Cre recombinase in the dorsal and ventral hippocampus (Fig. 6A) of $Scn1a^{fl/fl}$ mice, resulting in complete $Na_V1.1$ ablation, and $Scn1a^{fl/+}$ mice, to study also partial $Na_V1.1$ ablation (Fig. 6B) which may be more relevant in light of the haploinsufficiency observed in patients and $Scn1a^{-/+}$ DS mice. Within 28 days after injection, all $Scn1a^{fl/fl}$ mice and the majority of $Scn1a^{fl/+}$ mice developed interictal spikes (IIS; n = 6/6 and n = 6/7, respectively; Fig. 6D) and spontaneous seizures (n = 6/6 and n = 5/7, respectively; Fig. 6C,E), whereas neither were observed in WT controls injected with AAV-mCherry-Cre (n = 7). Statistical comparison indicated a significant increase in seizure count for $Scn1a^{fl/fl}$ and $Scn1a^{fl/+}$ mice when compared to controls (18.8 ± 6.8 and 9.4 ± 3.8 seizures, respectively; $H_{(2)} = 11.7$, $p < 0.05$, Kruskal-Wallis with Dunn's test), but seizure count did not differ significantly between the two genotypes ($p = 0.68$). Average onset of IIS was 11.5 days (range 9-14), while the first seizure was observed 13.1 days (range 10-18) after injection. Cortical theta-low gamma coupling was impaired already on day 7 after injection for $Scn1a^{fl/fl}$ mice (Fig. 6F,G). Also, theta-high gamma coupling was impaired at this time in $Scn1a^{fl/fl}$ and $Scn1a^{fl/+}$ mice (Fig. 6F,H). Modulation of both gamma frequency ranges did not recover over subsequent weeks (Fig. 6G,H). Power changes were limited to an increase in gamma power in $Scn1a^{fl/fl}$ mice on day 21 after injection ($1.5 \pm 0.1 \times 10^{-3}$ and $2.2 \pm 0.3 \times 10^{-3}$ mV^2/Hz, on day 2 and 21, respectively; $t_{(6)} = 3.1$, $p = 0.042$, paired t-test). These data indicate that attenuation of cortical theta-gamma coupling precedes IIS and spontaneous seizures following hippocampal deletion of $Na_V1.1$, independent of changes in power spectral density.

FIGURE 6. Chronic seizure activity following hippocampal ablation of $Na_V1.1$ is preceded by decreases in cortical theta-gamma coupling.

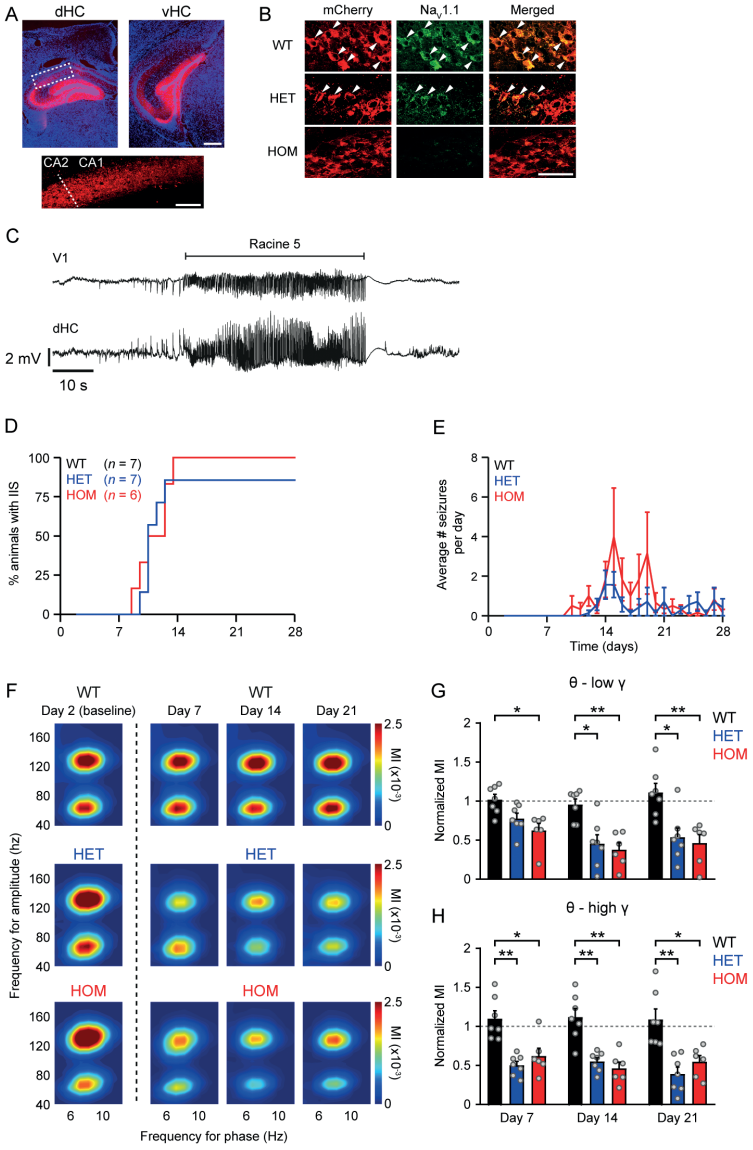

(A) Example of dorsal and ventral hippocampal areas (dHC and vHC, respectively) infected by AAV-mCherry-Cre (red; Hoechst in blue). Scale bar 500 µm. The targeted area included the CA1 and 2 region (boxed area expanded in bottom inset; dashed line indicates border CA1/2; scale bar 200 µm). **(B)** Detail of hippocampal CA1/2 region showing reduced $Na_V1.1$ staining in cells infected by AAV-mCherry-Cre (arrowheads indicate double-labeled cells) in *Scn1a*$^{fl/+}$ (HET) and *Scn1a*$^{fl/fl}$ (HOM) when compared to wildtype (WT). Scale bar 50 µm. **(C)** Spontaneous seizure in a HOM mouse on day 19 after hippocampal AAV-mCherry-Cre (V1 = primary visual cortex). **(D)** Proportion of HET ($n = 7$) and HOM ($n = 6$) mice with interictal spikes (IIS), after hippocampal AAV-mCherry-Cre on day 0. No IIS were observed in WT ($n = 7$). **(E)** Average frequency of spontaneous seizures following AAV-mCherry-Cre. **(F)** Average phase-amplitude comodulograms of V1 at different time points after injection. **(G,H)** Modulation index (MI), normalized to values obtained on day 2, was significantly decreased for both low gamma (γ; 40-90 Hz; G) and high gamma (90-160 Hz; H) frequencies in HET and HOM mice, when compared to WT mice ($F_{(2,17)} = 14.5$ and $F_{(2,17)} = 24.9$, respectively, $^*p < 0.05$, $^{**}p < 0.005$; two-way ANOVA with Tukey's test).

Attenuation of theta-high gamma coupling occurs independently of seizures following cortical-specific knock-out of *Scn1a*

In DS mice, both hippocampal and cortical regions may contribute to seizures,[15] and inhibitory dysfunction has been demonstrated in both structures.[3, 8] We therefore studied the effect of local cortical knock-out of *Scn1a* by injecting AAV-mCherry-Cre in V1 in *Scn1a*$^{fl/+}$ and *Scn1a*$^{fl/fl}$ mice, and WT controls (Fig. 7A,B). Interestingly, all *Scn1a*$^{fl/fl}$ mice developed IIS during the recording period, whereas this was the case for only a subset of *Scn1a*$^{fl/+}$ mice (n = 6/6 and n = 2/7, respectively; Fig. 7D). Spontaneous seizures were observed in a subset of *Scn1a*$^{fl/fl}$ mice (n = 2/6), but never in *Scn1a*$^{fl/+}$ mice (Fig. 7E). Previously, we reported a higher incidence of seizures in *Scn1a*$^{fl/fl}$ mice (n = 6/6) following cortical injections with an AAV vector expressing GFP-Cre under the CMV promotor.[15] As the discrepancy with our current data suggests a greater potency of the latter AAV vector, we tested whether this vector (AAV-GFP-Cre) would result in seizures following cortical injections in 6 *Scn1a*$^{fl/+}$ mice. Again, none of the *Scn1a*$^{fl/+}$ mice developed seizures, indicating that homozygous, but not heterozygous, knock-out of *Scn1a* in V1 predisposes animals to develop spontaneous seizures. Early attenuation of theta-gamma coupling, evident 7 days after injection, was restricted to the high gamma frequency range and persisted in *Scn1a*$^{fl/fl}$ mice but recovered in *Scn1a*$^{fl/+}$ (Fig. 7F-H). Power changes were limited to an increase in gamma power in *Scn1a*$^{fl/+}$ mice on day 21 after injection ($1.8 \pm 0.2 \times 10^{-3}$ and $2.4 \pm 0.2 \times 10^{-3}$ mV^2/Hz, on day 2 and 21, respectively; $t_{(6)} = 12.1$, $p < 0.0001$, paired t-test), while theta peak frequency was decreased in both *Scn1a*$^{fl/+}$ and *Scn1a*$^{fl/fl}$ on day 21 (difference of -0.2 ± 0.1 and -0.4 ± 0.1 Hz, respectively; $t_{(6)} = 2.6$, $p = 0.038$, and $t_{(5)} = 3.9$, $p = 0.012$, paired t-test). These observations suggest that cortical $Na_V1.1$ is required for modulation of high gamma by theta.

Hippocampal fast ripples and attenuated theta-gamma coupling precede epilepsy onset following hippocampal-specific knock-out of *Scn1a*

In addition to cortical LFP, mice that were injected in the hippocampus had local LFP recorded from AAV injection sites. Hippocampal theta-gamma coupling, theta and gamma power, and theta peak frequency decreased over time following injection in both *Scn1a*$^{fl/+}$ and *Scn1a*$^{fl/fl}$ mice (Fig. 8) and comodulograms showed modulation of different gamma frequency ranges, including those above 150 Hz (Fig. 9A). Interestingly, the gamma frequency range that showed the strongest modulation by theta phase decreased over time following local *Scn1a* knock-out (Fig. 8A and Fig. 9A). As such, the decrease in theta-gamma coupling (Fig. 8B) was caused by a strong reduction in theta-modulated high gamma, while low gamma was not significantly affected (Fig. 8C,D).

FIGURE 7. Cortical ablation of $Na_V1.1$ specifically decreases theta-high gamma coupling.

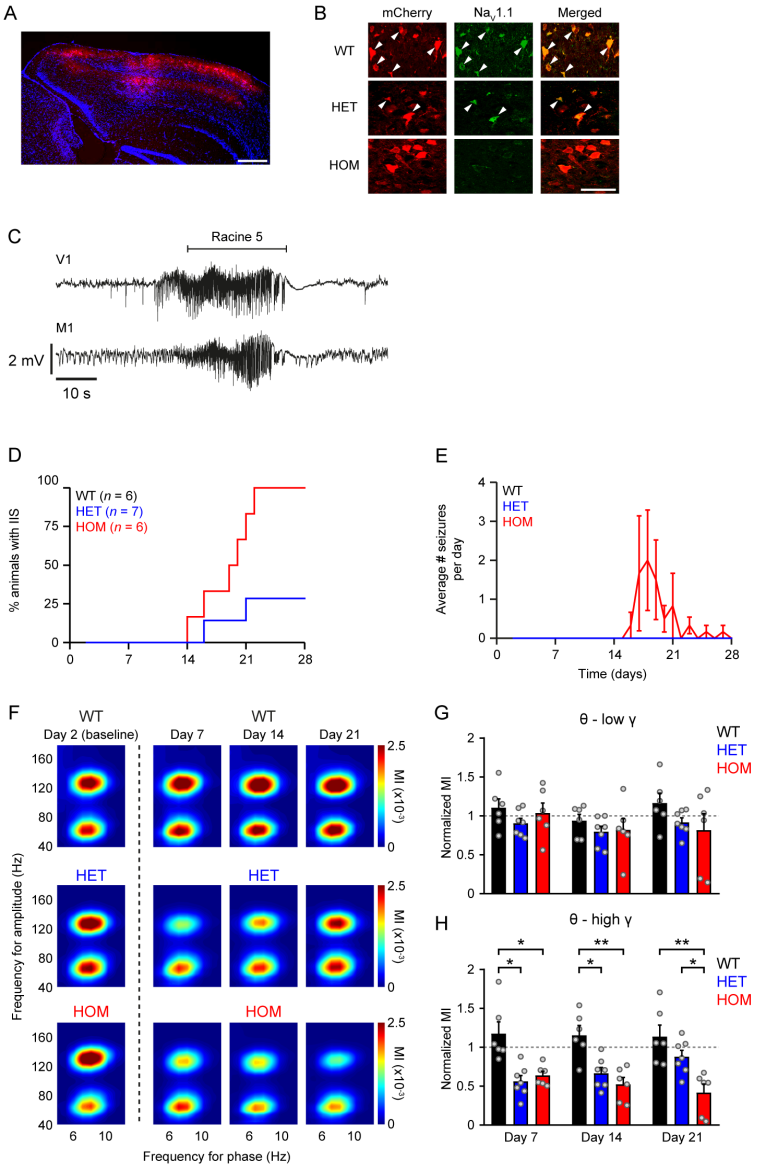

(A) Example of the primary visual cortex (V1) area infected by AAV-mCherry-Cre (red; Hoechst in blue). Scale bar 500 µm. **(B)** Detail of V1 showing reduced $Na_V1.1$ staining in cells infected by AAV-mCherry-Cre (arrowheads indicate double-labeled cells) in *Scn1a*$^{fl/+}$ (HET) and *Scn1a*$^{fl/fl}$ (HOM) when compared to wildtype (WT). Scale bar 50 µm. **(C)** Spontaneous seizure recorded in an *Scn1a*$^{fl/fl}$ mouse on day 18 after cortical AAV-mCherry-Cre (M1 = primary motor cortex). **(D)** Proportion of HET (n = 7) and HOM (n = 6) mice with interictal spikes (IIS), following cortical AAV-mCherry-Cre on day 0. No IIS were observed in WT mice (n = 6). **(E)** Average frequency of spontaneous seizures following injection of AAV-mCherry-Cre. **(F)** Average phase-amplitude comodulograms of V1 at different time points after injection. **(G,H)** Modulation index (MI), normalized to values obtained on day 2, was significantly decreased for high gamma (γ; H), but not low gamma, in HET and HOM mice when compared to WT mice ($F_{(2,16)}$ = 18.5 and $F_{(2,16)}$ = 1.3, respectively, *p < 0.05, **p < 0.005; two-way ANOVA with Tukey's test).

FIGURE 8. Deficient hippocampal theta-gamma coupling and power following local ablation of $Na_V1.1$.

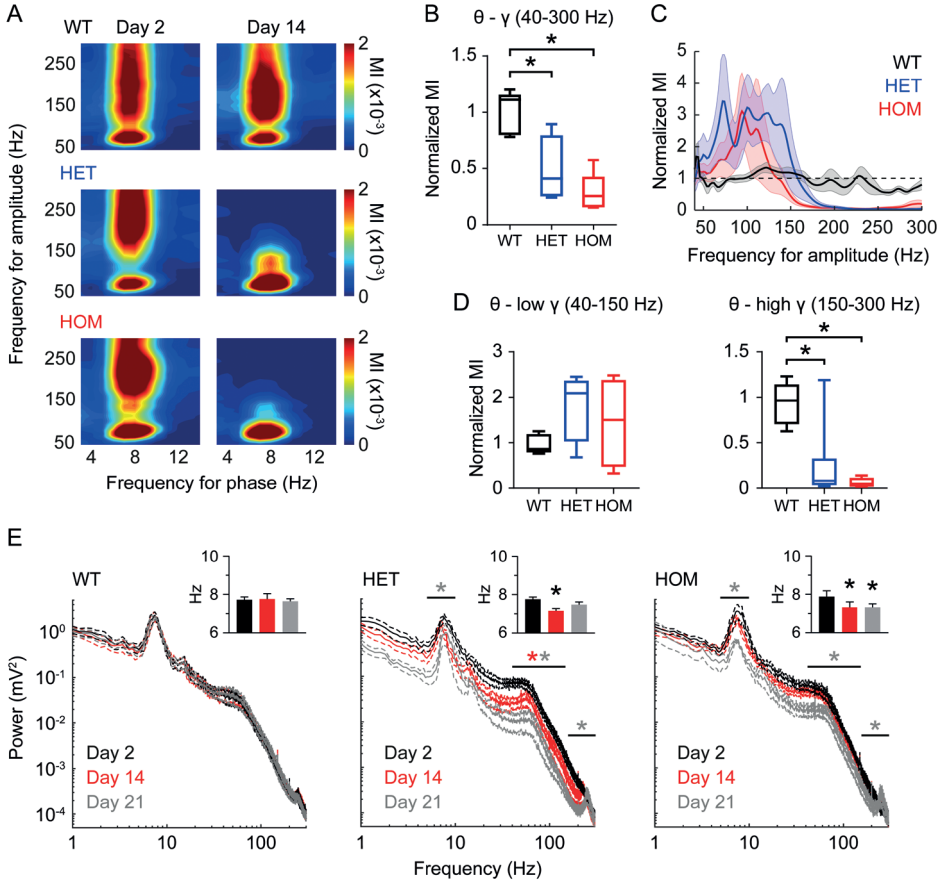

(A) Average phase-amplitude comodulograms of LFP obtained from dorsal hippocampus during day 2 (left) and 14 (right) after hippocampal injection of mCherry-Cre. **(B)** Theta-gamma coupling was reduced in *Scn1a*$^{fl/+}$ and *Scn1a*$^{fl/fl}$ mice on day 14 (total theta-gamma modulation index [MI] normalized to day 2; $F_{(2,17)} = 13.9$, $^*p < 0.01$, one-way ANOVA with Dunnett's test). **(C)** MI normalized per 2-Hz gamma (γ) frequency bin revealed that MI was specifically reduced for gamma frequencies >150 Hz, while showing large variation for the lower gamma range. **(D)** Statistical comparison revealed no difference for theta-modulated low gamma ($F_{(2,17)} = 1.3$, $p = 0.31$), but a significant reduction for high gamma ($F_{(2,17)} = 11.4$, $p = 0.001$) for both *Scn1a*$^{fl/+}$ and *Scn1a*$^{fl/fl}$ mice ($^*p = 0.004$ and $^*p = 0.001$, ANOVA with Dunnett's test). **(E)** Hippocampal LFP power spectral density during REM sleep in wildtype (WT, $n = 7$), *Scn1a*$^{fl/+}$ (HET, $n = 7$) and *Scn1a*$^{fl/fl}$ (HOM, $n = 6$) mice during day 2 (black), 14 (red) and 21 (grey) after hippocampal injection of mCherry-Cre. Power was significantly reduced only in HET and HOM mice. Asterisks of corresponding color indicate significant differences of power in theta (5-10 Hz), low gamma (40-150 Hz) or high gamma (150-300 Hz) on day 2 ($^*p < 0.05$, paired *t*-tests).

Hippocampal fast ripples (250-500 Hz) appear to occur specifically in the seizure onset zone,[41] independent of cell loss associated with hippocampal sclerosis.[42] To study the association between fast ripples and local theta-gamma coupling following hippocampal-specific knock-out of *Scn1a*, we inspected hippocampal LFP recordings for fast ripples over 12 hours preceding the first spontaneous seizure. In 7 out of 13 animals (n = 3 *Scn1a*$^{fl/+}$ and n = 4 *Scn1a*$^{fl/fl}$ mice), we found fast ripples that were superimposed on interictal discharges (Fig. 9B) in either the ventral (n = 4) or dorsal (n = 3) hippocampus. Following exclusion of one animal with bilateral fast ripples, comparison of hippocampal theta-gamma coupling ipsi- and contralateral to the fast ripples revealed a profound reduction in average MI for the ipsilateral electrode (Fig. 9C). The difference between baseline and preictal MI was also significantly greater for the ipsilateral compared to the contralateral electrode ($-7.8 \pm 1.5 \times 10^{-4}$ and $-2.1 \pm 0.6 \times 10^{-4}$, respectively; p = 0.002, Mann-Whitney test). Similarly, the gamma frequency that showed the strongest modulation by theta phase was decreased in the hours preceding seizure activity, specifically for the ipsilateral electrode (Fig. 9D). The drop in gamma frequency between baseline and the preictal period was not significantly different between sides (-79 ± 19 Hz and -36 ± 18 Hz for ipsi- and contralateral, respectively; p = 0.14, Mann-Whitney test). These data confirm theta-gamma coupling as a marker for epileptogenesis in these mice, as its attenuation precedes the first spontaneous seizure in an area corresponding to the seizure onset zone.

FIGURE 9. Theta-gamma coupling is affected more in areas that show fast ripples following hippocampal $Na_V1.1$ ablation.

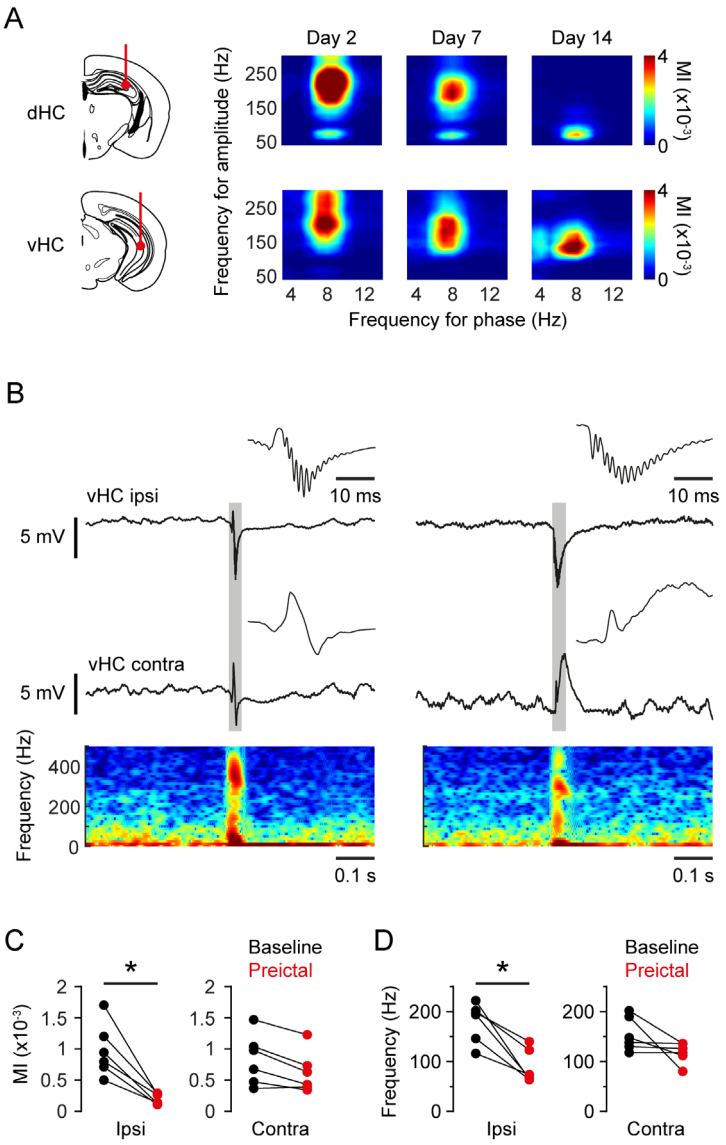

(A) Example phase-amplitude comodulograms of LFP in the dorsal and ventral hippocampus (dHC and vHC, respectively) following hippocampal injection of AAV-mCherry-Cre on day 0 in an *Scn1a*$^{fl/fl}$ mouse. **(B)** Examples of fast ripples observed in the ventral hippocampus of an *Scn1a*$^{fl/fl}$ (left) and *Scn1a*$^{fl/+}$ (right) mouse. Fast ripples (detailed in insets, corresponding to the shaded area) were observed unilaterally (vHC ipsi) and had a high power in the 250-500 Hz range, as shown by the spectrogram of the ipsilateral vHC signal at the bottom. Their onset preceded or coincided with interictal spikes on the contralateral side (vHC contra). **(C)** For hippocampal LFP that contained fast ripples (ipsi), theta-gamma coupling, assessed by the modulation index (MI; averaged for the total gamma frequency range [40-300 Hz]), was significantly decreased in the 12 hours preceding the first seizure (preictal) when compared to day 2 after injection (baseline; $*p = 0.031$, Wilcoxon test). In parallel, the gamma frequency showing peak MI was significantly reduced (**D**; $p = 0.031$, Wilcoxon test). MI changes of contralateral LFP that did not contain fast ripples (contra) did not reach statistical significance.

Impairment of voltage-gated sodium currents in inhibitory neurons attenuates theta-gamma coupling and theta frequency in a computational model

Our *in vivo* experiments indicate that theta-gamma coupling decreases prior to the first spontaneous seizure, suggesting that epilepsy-related remodeling is not responsible for this deficit in network functioning. To test whether decreased theta-gamma coupling may result from loss of voltage-gated sodium currents in inhibitory neurons, we developed a hippocampal network model in which we varied the amount of voltage-gated sodium channel (Na_V) function by decreasing their sodium conductance in modified Hodgkin–Huxley neurons representing fast-spiking basket cell (BC) neurons[43] and oriens-lacunosum moleculare (OLM) neurons.[44] Synaptic connections between BC, OLM and pyramidal (EX) neurons were all-to-all (Fig. 10A) and five neurons of each type were included in the model. LFP generated by the model was dominated by theta oscillations both at baseline (BC: 10 mS/cm^2, OLM: 35 mS/cm^2) and after decreasing sodium conductance in inhibitory neurons (BC: 6 mS/cm^2, OLM: 28 mS/cm^2; Fig. 10B). Theta peak frequency however was shifted to the left in case of impaired Na_V function when compared to baseline, while power in the gamma range was comparable (9.49×10^{-5} and 9.51×10^{-5}, respectively; Fig. 10C). Modulation of gamma by theta was present in both conditions, but reduced in case of impaired Na_V function, which was most evident for gamma oscillations >100 Hz (Fig. 10D). Impairment of inhibitory Na_V function in this computational model thus faithfully replicates both the reduced theta frequency and reduced theta-gamma coupling observed in DS mice.

To delineate the specific roles of the two populations of inhibitory interneurons in this model, we next systematically decreased Na_V function in either BC or OLM neurons. We found that the leftward shift in theta power results from Na_V dysfunction in the OLM population (Fig. 10E). Decreasing Na_V function in BC or OLM neurons had opposite effects on theta-gamma coupling: decreasing Na_V function in BC neurons alone impaired theta-gamma MI, while decreasing Na_V function in OLM neurons increased MI (Fig. 10F). Simultaneous reduction of Na_V function in both BC and OLM neurons resulted in a progressive decrease in theta-gamma MI over the high gamma (100-200 Hz) range, while a slight increase followed by a decrease occurred over the low gamma (40-100 Hz) range. Thus, theta-modulated high gamma is more strongly affected than low gamma in this computational model, which reproduces the *in vivo* results obtained following local *Scn1a* knock-out.

FIGURE 10. Modeling impaired Na_V functioning in inhibitory neurons replicates the attenuated theta-gamma coupling and decreased theta frequency observed after ablation of $Na_V1.1$.

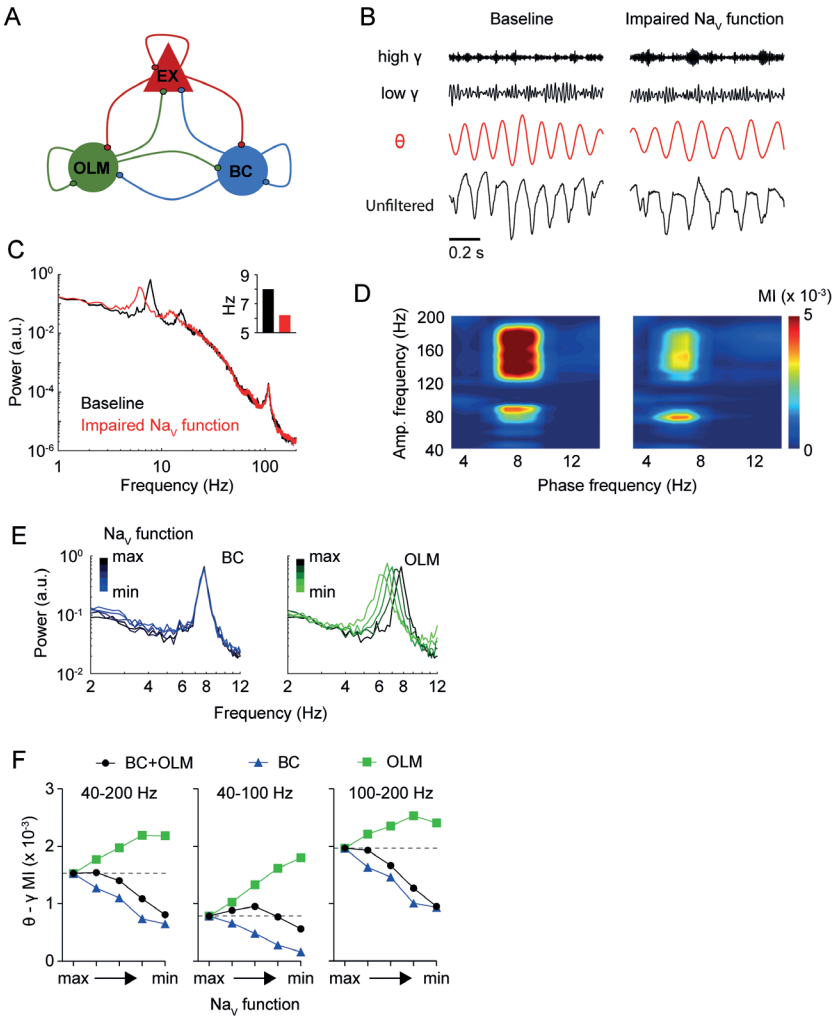

(A) Schematic of the computational network consisting of 5 pyramidal (EX), oriens-lacunosum moleculare (OLM) and fast-spiking basket cell (BC) neurons each with all-to-all connectivity. Full details about the model are provided in Figure 10-1. **(B)** Example traces of raw, theta-filtered (θ; 5-10 Hz), low gamma-filtered (low γ; 40-100 Hz), and high gamma (high γ; 100-200 Hz) filtered local field potential (LFP) from the model with normal (baseline) and impaired Na_V function in both OLM neurons (35 and 28 mS/cm^2, respectively) and BC neurons (10 and 6 mS/cm^2, respectively). **(C)** Average LFP power spectra from the same simulations used in **(B)** with normal (black) or impaired (red) inhibitory Na_V function, showing intact gamma power and a reduced theta peak frequency in the latter (C, inset). **(D)** Phase-amplitude comodulograms of these simulations show impaired theta-modulated gamma. **(E)** Stepwise impairment of Na_V function specifically in BC neurons (blue, left plot) or OLM neurons (green, right plot) resulted in a leftward shift in peak theta frequency for OLM neurons (black: 35 mS/cm^2, bright green: 28 mS/cm^2, steps of 1.75 mS/cm^2), but not for BC neurons (black: 10 mS/cm^2, bright blue: 6 mS/cm^2, steps of 1 mS/cm^2). **(F)** Average theta-gamma modulation index (MI) calculated for total gamma (left), low gamma (center), and high gamma (right) with decreasing levels of Na_V function in BC neurons (blue), OLM neurons (green) and both BC and OLM neurons (black).

DISCUSSION

We here report in juvenile DS mice impaired theta-gamma phase-amplitude coupling, that persisted in mice that developed spontaneous seizures but recovered to WT levels in mice that remained seizure-free. Impaired theta-gamma coupling was improved following acute CBD treatment. Hippocampal or cortical-specific knock-out of *Scn1a* impaired cortical theta-gamma coupling, which preceded spontaneous seizures. Attenuated modulation of high gamma by theta in the hippocampus, which colocalized with fast ripple activity preceding the start of chronic epileptic activity, was reproduced in a computational model in which Na_V dysfunction was selectively introduced in inhibitory neurons. Together, our findings indicate that theta-gamma coupling may serve as an early indicator of inhibitory dysfunction and epileptogenesis in DS.

Dysfunction of inhibitory interneurons has been demonstrated in DS mouse models,[7, 8, 45, 46] and may depend on age window or brain region.[47, 48] Reports on how inhibitory dysfunction affects network dynamics in DS mice appear more ambiguous. For instance, decreased delta power during non-REM sleep was reported in DS mice,[17] but changes in sleep-related delta power were not present in another DS model.[49] Also, interneurons were hypoexcitable, but LFP power was unchanged in DS mice during the pre-epileptic period.[7] Clinically, patients with DS often have a normal background EEG at 1 to 2 years of age, while seizures already manifest at this time.[50, 51] We did not detect differences in theta or gamma power during REM sleep and active wakefulness in DS *versus* WT mice. This contrasts with a previous study reporting decreased theta power during REM sleep in DS mice,[17] which may be explained by differences in mouse strain background and the cortical area studied. Also, we used a strict cutoff in theta/delta ratio to delineate epochs of REM sleep and active wakefulness, which may have rendered our analyses less sensitive to subtle differences in theta power. Nevertheless, our results indicate that theta-gamma coupling is a more sensitive measure of network dysfunction in DS than power spectral density.

Knock-out of *Scn1a* appears to specifically affect inhibitory populations, with reduced sodium currents lowering their excitability,[3, 5, 8, 47] although increased sodium currents have been reported in hippocampal excitatory neurons.[52] Such hyperexcitability of hippocampal excitatory neurons may be attributed to seizure-induced remodeling in DS mice.[35, 53] Importantly, chronic epilepsy may impair theta-gamma coupling, as demonstrated for the hippocampal CA1 region in a rat model of temporal lobe epilepsy.[54] Similarly, impairments in theta-gamma coupling were recently found in the hippocampus of rats following local knock-down of *Scn1a*, whereas no epileptiform activity was observed.[14] Although such activity may not be detected since recordings were performed during wakefulness, when IIS are rare,[17] $Na_V1.1$ dysfunction was induced only in CA1 of the dorsal hippocampus,[14] which may prove insufficient to cause epileptiform activity. In our study, the majority of the hippocampus was targeted, such that subregional effects of $Na_V1.1$ dysfunction cannot be discerned. DS mice and mice with local hippocampal or cortical knock-out of *Scn1a* showed early impairment of theta-gamma coupling before, or in the absence of, chronic epileptic activity. This impairment was transient in seizure-free DS mice, but persisted in mice with

spontaneous seizure activity. Thus, our data indicate that theta-gamma coupling is impaired early in *all* DS mice, but persistence of impaired theta-gamma coupling at later stages is dependent on seizure-induced network remodeling.

Over postnatal weeks 4 to 7, WT and DS mice showed an increase in cortical theta-gamma coupling. In mice, this is a developmental period of high cortical plasticity that starts with maturation of fast-spiking parvalbumin-positive interneurons.[39,40] In seizure-free DS mice, we found that theta-gamma coupling is impaired at P23, but normalized to WT levels at P28-42. This evolution roughly corresponds to developmental data from cortical parvalbumin-positive interneurons that show decreased firing only at P18-21, but not at P35-56, suggesting that their dysfunction contributes to the onset, but not chronification, of epilepsy in DS.[47] Here, local cortical heterozygous knock-out of *Scn1a* resulted in transient attenuation of theta-gamma coupling, which may reflect such temporary inhibitory dysfunction. CBD, which increases inhibitory neurotransmission in DS mice,[37] increased theta-gamma coupling, supporting a link between inhibitory functioning and theta-gamma coupling. Evidence that theta rhythms modulate a greater proportion of inhibitory interneurons when compared to excitatory neurons[11,12] suggests that inhibitory dysfunction particularly impacts theta-gamma coupling. This is further attested by impaired modulation of hippocampal gamma amplitude by theta phase in mice that lacked inhibition onto parvalbumin-positive interneurons, while theta power and peak frequency was reduced.[13] Similarly, we found a reduced theta peak frequency in DS mice, and following local $Na_V1.1$ ablation. Decreased $Na_V1.1$ expression was also observed in a mouse model of Alzheimer's disease, as well as in patients, providing an explanation for dysfunction of parvalbumin-positive interneurons.[55] Since impaired theta-gamma coupling has been demonstrated in Alzheimer's models,[56,57] similar mechanisms may underlie such rhythmopathies in Alzheimer's disease and DS models.

In our computational model, decreases in theta peak frequency could be attributed to Na_V dysfunction in OLM neurons. In animal models of temporal lobe epilepsy, hippocampal theta frequency is decreased[58,59] and degeneration of OLM neurons, resulting in loss of dendritic inhibition, has been observed.[60] Thus, decreased theta frequency appears to be a general feature of the epileptic hippocampus, and dysfunction and/or loss of OLM neurons may underlie this phenomenon. Although (parvalbuminergic) BC neurons appear to maintain their function in the epileptic hippocampus,[60,61] dysfunction of these neurons has been related to impaired theta-gamma coupling,[54] which we confirmed here by modeling BC Na_V dysfunction. Together, our findings suggest that decreased theta frequency and theta-gamma coupling reflect the impaired inhibitory functioning observed in DS mice. Network dynamics underlying cross-frequency coupling, however, are complex, and different factors may affect theta-gamma coupling in other disease models.

We distinguished low and high gamma bands, supported by evidence that mechanisms underlying these oscillations are different.[9] High gamma (above 80-90 Hz) peaks at a different phase of the theta cycle than low gamma,[62] as confirmed by our data, and strongly correlates with neuronal spiking.[63] Local $Na_V1.1$ dysfunction impaired local theta-modulated high, but not low, gamma

oscillations, which was computationally replicated. This suggests that $Na_V1.1$ dysfunction impairs modulation of *local* neuronal firing by theta, as previously shown for CA1 neurons following local $Na_V1.1$ knock-down.[14] The critical role for fast-spiking BC in regulating spike timing by somatic inhibition[40] may explain these early deficits in theta-high gamma coupling.

Increased hippocampal theta-gamma coupling is associated with memory recall in rodents[64] and humans.[65, 66] Memory impairment is frequently observed in patients with temporal lobe epilepsy.[67, 68] Although we did not relate changes in theta-gamma coupling to learning, previous studies indicate that context-dependent and spatial memory are impaired in DS mouse models.[4, 35] Cognitive deficits were only present in adult DS mice that had experienced seizures at juvenile age,[35] which may be related to persistent deficits in theta-gamma coupling that we only observed in adult DS mice with juvenile-onset seizures. The hippocampus appears to critically contribute to spatial memory deficits and the epileptic phenotype in DS mice.[29, 30] Our data suggest that impaired theta-gamma coupling precedes seizures and associates unilaterally with fast ripple activity in the hippocampus, a marker for epileptogenesis.[41] Further studies are required to translate these findings to other epilepsy models. Reductions in theta frequency in such models have been suggested to underlie cognitive deficits in epilepsy,[59, 69] but in our experiments occurred regardless of epileptic activity. Similarly, local knock-down of $Na_V1.1$ in the medial septum, which provides input to the hippocampus, decreased theta frequency and disrupted spatial memory in rats[70] without inducing seizure activity,[71] indicating that regions other than the hippocampus may contribute to impaired spatial memory and theta rhythmogenesis in DS. To recapitulate rhythmopathies in DS, the precision of computational models may therefore be improved by including inputs such as provided by the medial septum.

REFERENCES

1. Wolff, M., C. Casse-Perrot, and C. Dravet, Severe myoclonic epilepsy of infants (Dravet syndrome): natural history and neuropsychological findings. *Epilepsia*, 2006. 47 Suppl 2: p. 45-8.
2. Dravet, C., The core Dravet syndrome phenotype. *Epilepsia*, 2011. 52 Suppl 2: p. 3-9.
3. Yu, F.H., et al., Reduced sodium current in GABAergic interneurons in a mouse model of severe myoclonic epilepsy in infancy. *Nat Neurosci*, 2006. 9(9): p. 1142-9.
4. Han, S., et al., Autistic-like behaviour in Scn1a+/- mice and rescue by enhanced GABA-mediated neurotransmission. *Nature*, 2012. 489(7416): p. 385-90.
5. Ogiwara, I., et al., Nav1.1 localizes to axons of parvalbumin-positive inhibitory interneurons: a circuit basis for epileptic seizures in mice carrying an Scn1a gene mutation. *J Neurosci*, 2007. 27(22): p. 5903-14.
6. Cheah, C.S., et al., Specific deletion of NaV1.1 sodium channels in inhibitory interneurons causes seizures and premature death in a mouse model of Dravet syndrome. *Proc Natl Acad Sci U S A*, 2012. 109(36): p. 14646-51.
7. De Stasi, A.M., et al., Unaltered Network Activity and Interneuronal Firing During Spontaneous Cortical Dynamics In Vivo in a Mouse Model of Severe Myoclonic Epilepsy of Infancy. *Cereb Cortex*, 2016. 26(4): p. 1778-94.
8. Tai, C., et al., Impaired excitability of somatostatin- and parvalbumin-expressing cortical interneurons in a mouse model of Dravet syndrome. *Proc Natl Acad Sci U S A*, 2014. 111(30): p. E3139-48.
9. Buzsaki, G. and X.J. Wang, Mechanisms of gamma oscillations. *Annu Rev Neurosci*, 2012. 35: p. 203-25.
10. Freund, T.F. and I. Katona, Perisomatic inhibition. *Neuron*, 2007. 56(1): p. 33-42.
11. Csicsvari, J., et al., Oscillatory coupling of hippocampal pyramidal cells and interneurons in the behaving *Rat. J Neurosci,* 1999. 19(1): p. 274-87.
12. Sirota, A., et al., Entrainment of neocortical neurons and gamma oscillations by the hippocampal theta rhythm. *Neuron*, 2008. 60(4): p. 683-97.
13. Wulff, P., et al., Hippocampal theta rhythm and its coupling with gamma oscillations require fast inhibition onto parvalbumin-positive interneurons. *Proc Natl Acad Sci U S A*, 2009. 106(9): p. 3561-6.
14. Sakkaki, S., et al., Focal Dorsal Hippocampal Nav1.1 Knock Down Alters Place Cell Temporal Coordination and Spatial Behavior. *Cereb Cortex*, 2020. 30(9): p. 5049-5066.
15. Jansen, N.A., et al., Focal and generalized seizure activity after local hippocampal or cortical ablation of NaV 1.1 channels in mice. *Epilepsia*, 2020. 61(4): p. e30-e36.
16. Racine, R.J., Modification of seizure activity by electrical stimulation. II. Motor seizure. *Electroencephalogr Clin Neurophysiol*, 1972. 32(3): p. 281-94.
17. Kalume, F., et al., Sleep impairment and reduced interneuron excitability in a mouse model of Dravet Syndrome. *Neurobiol Dis*, 2015. 77: p. 141-54.
18. Tort, A.B., et al., Measuring phase-amplitude coupling between neuronal oscillations of different frequencies. *J Neurophysiol*, 2010. 104(2): p. 1195-210.
19. Kopell, N., et al., Gamma and theta rhythms in biophysical models of hippocampal circuits, in *Hippocampal microcircuits*. 2010, Springer. p. 423-457.

20. Cressman, J.R., Jr., et al., The influence of sodium and potassium dynamics on excitability, seizures, and the stability of persistent states: I. Single neuron dynamics. *J Comput Neurosci*, 2009. 26(2): p. 159-70.
21. Hubel, N., et al., The role of glutamate in neuronal ion homeostasis: A case study of spreading depolarization. *PLoS Comput Biol*, 2017. 13(10): p. e1005804.
22. Ullah, G., The role of transporters and synaptic cleft morphology in glutamate and GABA homeostasis and their effect on neuronal function. *BioRxiv*, 2019: p. 670844.
23. Ullah, G. and S.J. Schiff, Assimilating seizure dynamics. *PLoS Comput Biol*, 2010. 6(5): p. e1000776.
24. Ullah, G., et al., The Role of Cell Volume in the Dynamics of Seizure, Spreading Depression, and Anoxic Depolarization. *PLoS Comput Biol*, 2015. 11(8): p. e1004414.
25. Wei, Y., G. Ullah, and S.J. Schiff, Unification of neuronal spikes, seizures, and spreading depression. *J Neurosci*, 2014. 34(35): p. 11733-43.
26. Scheffzuk, C., et al., Selective coupling between theta phase and neocortical fast gamma oscillations during REM-sleep in mice. *PLoS One*, 2011. 6(12): p. e28489.
27. Bandarabadi, M., et al., Dynamic modulation of theta-gamma coupling during rapid eye movement sleep. *Sleep*, 2019. 42(12).
28. Gerbrandt, L.K., et al., Origin of the neocortically monitored theta rhythm in the curarized rat. *Electroencephalogr Clin Neurophysiol*, 1978. 45(4): p. 454-67.
29. Liautard, C., et al., Hippocampal hyperexcitability and specific epileptiform activity in a mouse model of Dravet syndrome. *Epilepsia*, 2013. 54(7): p. 1251-61.
30. Stein, R.E., et al., Hippocampal deletion of NaV1.1 channels in mice causes thermal seizures and cognitive deficit characteristic of Dravet Syndrome. *Proc Natl Acad Sci U S A*, 2019. 116(33): p. 16571-16576.
31. Bragin, A., et al., Gamma (40-100 Hz) oscillation in the hippocampus of the behaving rat. *J Neurosci*, 1995. 15(1 Pt 1): p. 47-60.
32. Buzsaki, G., et al., Hippocampal network patterns of activity in the mouse. *Neuroscience*, 2003. 116(1): p. 201-11.
33. Schomburg, E.W., et al., Theta phase segregation of input-specific gamma patterns in entorhinal-hippocampal networks. *Neuron*, 2014. 84(2): p. 470-85.
34. Kalume, F., et al., Sudden unexpected death in a mouse model of Dravet syndrome. *J Clin Invest*, 2013. 123(4): p. 1798-808.
35. Salgueiro-Pereira, A.R., et al., A two-hit story: Seizures and genetic mutation interaction sets phenotype severity in SCN1A epilepsies. *Neurobiol Dis*, 2019. 125: p. 31-44.
36. Devinsky, O., et al., Trial of Cannabidiol for Drug-Resistant Seizures in the Dravet Syndrome. *N Engl J* Med, 2017. 376(21): p. 2011-2020.
37. Kaplan, J.S., et al., Cannabidiol attenuates seizures and social deficits in a mouse model of Dravet syndrome. *Proc Natl Acad Sci U S A*, 2017. 114(42): p. 11229-11234.
38. Deiana, S., et al., Plasma and brain pharmacokinetic profile of cannabidiol (CBD), cannabidivarine (CBDV), Delta(9)-tetrahydrocannabivarin (THCV) and cannabigerol (CBG) in rats and mice following oral and intraperitoneal administration and CBD action on obsessive-compulsive behaviour. *Psychopharmacology* (Berl), 2012. 219(3): p. 859-73.

39. Takesian, A.E. and T.K. Hensch, Balancing plasticity/stability across brain development. *Prog Brain Res*, 2013. 207: p. 3-34.
40. Cardin, J.A., Inhibitory Interneurons Regulate Temporal Precision and Correlations in Cortical Circuits. *Trends Neurosci*, 2018. 41(10): p. 689-700.
41. Jefferys, J.G., et al., Mechanisms of physiological and epileptic HFO generation. *Prog Neurobiol*, 2012. 98(3): p. 250-64.
42. Jiruska, P., et al., Epileptic high-frequency network activity in a model of non-lesional temporal lobe epilepsy. *Brain*, 2010. 133(Pt 5): p. 1380-90.
43. Wang, X.J. and G. Buzsaki, Gamma oscillation by synaptic inhibition in a hippocampal interneuronal network model. *J Neurosci*, 1996. 16(20): p. 6402-13.
44. Tort, A.B., et al., On the formation of gamma-coherent cell assemblies by oriens lacunosum-moleculare interneurons in the hippocampus. *Proc Natl Acad Sci U S A*, 2007. 104(33): p. 13490-5.
45. Rubinstein, M., et al., Genetic background modulates impaired excitability of inhibitory neurons in a mouse model of Dravet syndrome. *Neurobiol Dis*, 2015. 73: p. 106-17.
46. Goff, K.M. and E.M. Goldberg, Vasoactive intestinal peptide-expressing interneurons are impaired in a mouse model of Dravet syndrome. *Elife*, 2019. 8.
47. Favero, M., et al., A Transient Developmental Window of Fast-Spiking Interneuron Dysfunction in a Mouse Model of Dravet Syndrome. *J Neurosci*, 2018. 38(36): p. 7912-7927.
48. Almog, Y., Brusel, M., Anderson, K., Rubinstein, M., Early hippocampal hyperexcitability followed by disinhibition in a mouse model of Dravet syndrome. *bioRxiv*, 2019(790170).
49. Papale, L.A., et al., Altered sleep regulation in a mouse model of SCN1A-derived genetic epilepsy with febrile seizures plus (GEFS+). *Epilepsia*, 2013. 54(4): p. 625-34.
50. Bureau, M. and B. Dalla Bernardina, Electroencephalographic characteristics of Dravet syndrome. *Epilepsia*, 2011. 52 Suppl 2: p. 13-23.
51. Wirrell, E.C., et al., Optimizing the Diagnosis and Management of Dravet Syndrome: Recommendations From a North American Consensus Panel. *Pediatr Neurol*, 2017. 68: p. 18-34 e3.
52. Mistry, A.M., et al., Strain- and age-dependent hippocampal neuron sodium currents correlate with epilepsy severity in Dravet syndrome mice. *Neurobiol Dis*, 2014. 65: p. 1-11.
53. Dutton, S.B.B., et al., Early-life febrile seizures worsen adult phenotypes in Scn1a mutants. *Exp Neurol*, 2017. 293: p. 159-171.
54. Lopez-Pigozzi, D., et al., Altered Oscillatory Dynamics of CA1 Parvalbumin Basket Cells during Theta-Gamma Rhythmopathies of Temporal Lobe Epilepsy. *eNeuro*, 2016. 3(6).
55. Verret, L., et al., Inhibitory interneuron deficit links altered network activity and cognitive dysfunction in Alzheimer model. *Cell*, 2012. 149(3): p. 708-21.
56. Ittner, A.A., et al., p38 MAP kinase-mediated NMDA receptor-dependent suppression of hippocampal hypersynchronicity in a mouse model of Alzheimer's disease. *Acta Neuropathol Commun*, 2014. 2: p. 149.
57. Zhang, X., et al., Impaired theta-gamma coupling in APP-deficient mice. *Sci Rep*, 2016. 6: p. 21948.
58. Dugladze, T., et al., Impaired hippocampal rhythmogenesis in a mouse model of mesial temporal lobe epilepsy. *Proc Natl Acad Sci U S A*, 2007. 104(44): p. 17530-5.

59. Kilias, A., et al., Theta frequency decreases throughout the hippocampal formation in a focal epilepsy model. *Hippocampus*, 2018. 28(6): p. 375-391.
60. Cossart, R., et al., Dendritic but not somatic GABAergic inhibition is decreased in experimental epilepsy. *Nat Neurosci*, 2001. 4(1): p. 52-62.
61. Wittner, L., et al., Surviving CA1 pyramidal cells receive intact perisomatic inhibitory input in the human epileptic hippocampus. *Brain*, 2005. 128(Pt 1): p. 138-52.
62. Belluscio, M.A., et al., Cross-frequency phase-phase coupling between theta and gamma oscillations in the hippocampus. *J Neurosci*, 2012. 32(2): p. 423-35.
63. Ray, S. and J.H. Maunsell, Different origins of gamma rhythm and high-gamma activity in macaque visual cortex. *PLoS Biol*, 2011. 9(4): p. e1000610.
64. Tort, A.B., et al., Theta-gamma coupling increases during the learning of item-context associations. *Proc Natl Acad Sci U S A*, 2009. 106(49): p. 20942-7.
65. Axmacher, N., et al., Cross-frequency coupling supports multi-item working memory in the human hippocampus. *Proc Natl Acad Sci U S A*, 2010. 107(7): p. 3228-33.
66. Heusser, A.C., et al., Episodic sequence memory is supported by a theta-gamma phase code. *Nat Neurosci*, 2016. 19(10): p. 1374-80.
67. Vlooswijk, M.C., et al., Functional MRI in chronic epilepsy: associations with cognitive impairment. *Lancet Neurol*, 2010. 9(10): p. 1018-27.
68. Helmstaedter, C. and C.E. Elger, Chronic temporal lobe epilepsy: a neurodevelopmental or progressively dementing disease? *Brain*, 2009. 132(Pt 10): p. 2822-30.
69. Shuman, T., B. Amendolara, and P. Golshani, Theta Rhythmopathy as a Cause of Cognitive Disability in TLE. *Epilepsy Curr*, 2017. 17(2): p. 107-111.
70. Bender, A.C., B.W. Luikart, and P.P. Lenck-Santini, Cognitive Deficits Associated with Nav1.1 Alterations: Involvement of Neuronal Firing Dynamics and Oscillations. *PLoS One*, 2016. 11(3): p. e0151538.
71. Bender, A.C., et al., Focal Scn1a knockdown induces cognitive impairment without seizures. *Neurobiol Dis*, 2013. 54: p. 297-307.

SUPPLEMENTARY MATERIAL

Extended data

FIGURE 10 - 1. Currents and fluxes regulating membrane potential, ion concentrations and neurotransmitter homeostasis for the computational neuronal network model.